J.E. Schmitz[1#], J.D. Teepe[2#], Y. Hu[3], C.E. Smith[3,4], R.J. Fajardo[1], and Y.-H.P. Chun[5]*

[1]Department of Orthopaedics, RAYO, Carlisle Center for Bone and Mineral Imaging, School of Medicine, University of Texas Health Science Center at San Antonio, USA; [2]Dunn Dental Clinic, Lackland Air Force Base, San Antonio, TX, USA; [3]Department of Biologic and Materials Sciences, University of Michigan, Dental Research Lab, Ann Arbor, MI, USA; [4]Department of Anatomy & Cell Biology, McGill University, Montreal, PQ, Canada; and [5]Department of Periodontics, Dental School, University of Texas Health Science Center at San Antonio, 7703 Floyd Curl Drive, San Antonio, TX 78229, USA; [#]authors contributing equally to this publication; *corresponding author, chuny@uthscsa.edu

Estimating Mineral Changes in Enamel Formation by Ashing/BSE and MicroCT

ABSTRACT

Enamel formation produces the most highly mineralized tissue in the human body. The growth of enamel crystallites is assisted by enamel proteins and proteinases. As enamel formation progresses from secretory to maturation stages, the composition of the matrix with its mineral and non-mineral components dynamically changes in an inverse fashion. We hypothesized that appropriately calibrated micro-computed tomography (μCT) technology is suitable to estimate the mineral content (weight and/or density) and volume comparable in accuracy with that for directly weighed and sectioned enamel. Different sets of mouse mandibular incisors of C57BL/6 mice were used for dissections and μCT reconstructions. Calibration phantoms corresponding to the range of enamel mineral densities were used. Secretory-stage enamel contained little mineral and was consequently too poor in contrast for enamel volumes to be accurately estimated by μCT. Maturation-stage enamel, however, showed remarkable correspondence for total mineral content *per* volume where comparisons were possible between and among the different analytical techniques used. The main advantages of the μCT approach are that it is non-destructive, time-efficient, and can monitor changes in mineral content of the most mature enamel, which is too physically hard to dissect away from the tooth.

KEY WORDS: enamel biomineralization/formation, mineralized tissue/development, micro-computed tomography, dental enamel, tooth, minerals, hydroxyapatite.

INTRODUCTION

Among the mineralized tissues of the human body, enamel has the highest concentration of mineral. Although mature enamel consists almost solely of hydroxyapatite, it does contain minute amounts of non-mineral components in the form of residual organic material and water (enamel fluid) within residual microspaces. This composition provides the unique durability and resistance to mature enamel needed to resist occlusal forces during mastication. Both the volume and the quantity of mineral present in enamel are controlled by columnar ameloblasts of epithelial origin. The prerequisites for mineralization events are the deposition of both enamel proteins and proteinases (Caterina *et al.*, 2002; Fukumoto *et al.*, 2004; Hu *et al.*, 2008; Simmer *et al.*, 2009; Smith *et al.*, 2011). During the secretory stage, the enamel layer gains simultaneously in volume and in mineral content through the apposition, cleavage, and removal of enamel proteins, and the elongation of crystallites (Smith *et al.*, 1989). The volume and shape of the enamel layer are controlled by ameloblasts that outline a confined space against the mineralized dentin. The initial precipitation and later volumetric growth of hydroxyapatite crystallites during the maturation stage are monitored by ameloblasts through pathways of ion metabolism (Smith, 1998; Lacruz *et al.*, 2013). The removal of organic material and the accumulation of mineral across the plasma membrane of ameloblasts are coupled (Smith and Nanci, 1996), and culminate in fully mature enamel (Smith *et al.*, 1989).

Direct measurements of mineral content and enamel volume are complicated, since enamel is bonded to the dentin to form a bilayered biomineral across the crown of the tooth. Invasive and non-invasive means have been devised to determine these parameters. A validated model for forming enamel and ameloblast stages is the rodent incisor in combination with microdissection of enamel, since it displays all developmental stages as it erupts continuously (Robinson *et al.*, 1971, 1977; Smith and Nanci, 1989). In this approach, enamel is lifted from dentin in 1-mm–wide strips from secretory through maturation stages (Smith and Nanci, 1989). Weight changes measured before and after heating to a specific temperature (ashing) provide information on the mineral and non-mineral content related to normal and pathological conditions during the course of amelogenesis (Smith *et al.*, 2009). This technique is destructive, extremely time-consuming, and lacks reproducible inter-examiner demands on hand-skills.

Micro-computed x-ray tomography (μCT) is a non-destructive method that exploits differences in x-ray intensity before and after passing through an object (Zou *et al.*, 2011). Differences in x-ray attenuation represent an object's density, but thickness can affect these assessments as well (Fajardo *et al*., 2009). During assessment of mineral density, the attenuation differences of an object are converted to generate an image, and each pixel is assigned a grayscale value corresponding to the linear attenuation coefficient (LAC). From the LAC, the density of an object at any location can be calculated (Fajardo *et al.*, 2002). In the past, the enamel had to be thinly sectioned for a 2-dimensional (2D) image to be obtained, but current desktop μCT systems can reconstruct intact objects in 3 dimensions with microscopic pixel sizes. The validity of density measurements relies on calibration with high-density hydroxyapatite (HA) standards (= phantoms) (Schweizer *et al*., 2007). It is technically challenging to fabricate phantoms of densities comparable with those of enamel because, at these high densities, the material is predominantly mineral, and specialized equipment is required to bond the crystals at high heat and/or high pressure. In the past, investigators were forced to assume that enamel mineral is equivalent to stoichiometric HA or to derive enamel density from chemical formulations (Angmar *et al.*, 1963; Robinson *et al.*, 1971; Elliott *et al.*, 1998). Until recently, the ashing method, which is considered the gold standard, and μCT have not been compared for enamel. The hypothesis of this study was that the volume, mineral weight, and mineral density of forming enamel can be analyzed by calibrated polychromatic μCT technology and that results from μCT correspond well to direct measurements done by ashing of enamel strips and backscattered electron microscopy.

MATERIALS & METHODS

Protocol Approval

Protocols for the use and handling of animals were approved by the IACUC of the University of Texas Health Science Center at San Antonio and the University of Michigan. This study complied with ARRIVE guidelines for pre-clinical studies.

Animals

In total, 23 wild-type mice (C57BL/6 background) at 7 wks old were used. They were fed hard chow (7012 Teklad L-M485, Harlan Laboratories, Indianapolis, IN, USA) and maintained on a standard 12-hour light/dark cycle. Animals for μCT scanning were intracardially perfused with 4% paraformaldehyde (PFA) in phosphate-buffered saline (PBS) with 0.2% glutaraldehyde, pH 7.4, and the hemi-mandibles were removed and stored at 4°C in PBS containing 0.2% PFA, pH 7.4. Hemi-mandibles from different animals were used for sections (n = 3), ash weight (n = 12), and μCT (n = 8) experiments (Appendix Fig. 1).

Microdissection, Ashing, Sectioning, and Calculation of Enamel Mineral Density

Data on enamel mineral weights *per* mm and the ashing technique used to obtain them have been reported previously (Smith *et al.*, 2009). To estimate enamel volumes *per* mm, we embedded hemi-mandibles from 3 wild-type mice in epoxy resin and cut them into eight 1-mm–long segments, starting near the apical loop. Enamel segments (ES) containing the incisor cross-sections were polished with up to 1,200-grit carbide paper and finished with a diamond suspension having a particle size of 1 μm (South Bay Technology, San Clemente, CA, USA). Images of the incisor cross-sections were obtained in backscattered mode with a Hitachi S-3000 N scanning electron microscope (15 kV, 20 Pa) (BSE). The area of the enamel was outlined (CellSens, Olympus, Center Valley, PA, USA), and the enamel volumes were calculated between 2 cross-sections in 1-mm intervals (= integrated volume). We calculated mineral density *per* mm by dividing ashed mineral weight by the volume estimated from the BSE measurements for the same location.

μCT Scanning, Object Reconstruction, Contouring of Enamel, and Calibration

Hemi-mandibles with attached soft tissues were scanned in 70% ethanol in a desktop SkyScan 1172 (Bruker SkyScan, Aartselaar, Belgium) system. Each specimen was positioned with the incisal edge pointing superiorly, and the tube was sealed with Parafilm (American National Can, Greenwich, CT, USA). Samples were scanned at 60 kV, 167 μA beam intensity, 5-μm image pixel size, a 0.35° rotation step, 7 frame averaging, and a 1,090-millisecond exposure time at each step. A 0.5-mm aluminum filter was used during scans (Kovács *et al.*, 2009). A polynomial correction was also used to reduce beam-hardening effects during reconstructions (Kovács *et al.*, 2009; Zou *et al*., 2011). These 2 protocols reduced the beam-hardening artifact (Appendix Figs. 2, 3). The images were reconstructed with NRecon (Bruker SkyScan, Aartselaar, Belgium) with a Feldkamp cone-beam algorithm (Feldkamp *et al.*, 1984).

Successive 1-mm–long volumes of interest were created, starting at 75% of the distance between the opening of the apical foramen and the distal boundary of the last mandibular molar at the level of the cement-enamel junction (Fig. 1B). In each volume of interest (VOI), the enamel boundary was manually outlined, with non-enamel objects excluded. Volumes of interest correspond to ES. Enamel volumes were determined from the manually drawn volumes of interest. Intra-operator error and inter-operator differences in volumes of interest were determined for the early, mid-, and late maturation stages (Appendix Table 1). HA phantoms (0.25 and 0.75 g/cm^3 (SkyScan), and 2.927 g/cm^3 (Himed, Bethpage, NY, USA) were used to calibrate mineral density analyses (Appendix Table 2; Appendix Fig. 4).

Volumetric Percent of Mineral and Non-mineral Components

Parameters that were directly measured from mice included the (1) gross weight of enamel mineral *per* mm (by ashing), (2) enamel volume *per* mm (by BSE), and (3) mineral density and estimated enamel volume *per* mm (by μCT). Several derived values were also calculated, as explained in the footnotes to the Table.
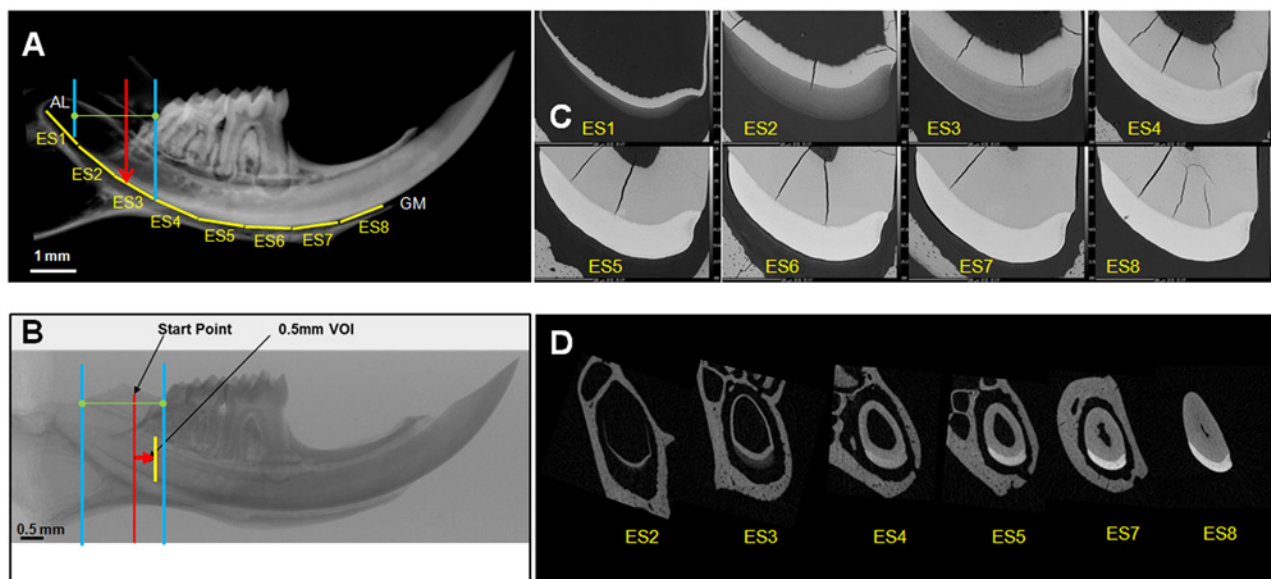
Figure 1. Enamel of mouse mandibular incisors gains thickness and mineral density (from left to right). **(A)** Hemi-mandibles in seven-week-old mice are a little over 11 mm in total length. The region containing developing enamel was sawed into eight 1-mm–long cross-sectional ESs (yellow horizontal lines, ES1-8) from near the apical loop (AL) to the gingival margin (GM). The average volumes *per* ES were then estimated from sequential area measurements of the cross-sectioned enamel faces. **(B)** For µCT, a series of 0.5-mm-long enamel volumes of interest (VOI) started at 75% of the distance between the apical loop (blue line, left) and the distal aspect of the third molar crown (blue line, right). From the start point (red line), the first VOI (yellow line) was generated (red arrow). **(C)** Examples of eight 1-mm–long ESs imaged by BSE. **(D)** Examples of µCT reconstructed trans-axial images of incisor enamel.

Statistical Analyses

Means and standard deviations were calculated in Excel and GraphPad InStat (La Jolla, CA, USA). Unpaired *t* tests and analyses of variance (ANOVAs) were used to compare volume and mineral density measurements. Paired *t* tests were used to assess inter-operator differences. The intra-operator error was expressed by the coefficient of variation. Alpha was set to 0.05.

RESULTS

Enamel Volume

Incisor enamel volume increased across the secretory stage (ES1-2), as seen in BSE images (Fig. 1). Sectioned and µCT-imaged enamel volumes showed overall agreement; the µCT-based enamel volumes were 4 to 12% lower than the sectioned volume estimates (Fig. 2). Volume peaked in the mid-maturation stage (ES4) for sectioned and µCT-based analyses (Table). Across the maturation stage, enamel volume shrank steadily, losing about 5% to 8% of total volume in the most mature enamel (ES8).

Enamel Mineral Weight, % Mineral, and % Non-mineral Components

Mineral weight measured from enamel strips ranged between 2.27 ± 1.45 µg (ES1) and 133.54 ± 20.95 µg (ES5). The enamel could not be dissected from the underlying dentin after ES5; the enamel was too hard to remove. The mineral content by volume increased from 20.69% (ES1) to 61.77% (ES5), with the greatest

accumulation occurring after the secretory stage when the ameloblasts transitioned into maturation stage. The percentage of non-mineral components by volume correspondingly decreased from 79.31% in ES1 to 38.23% in ES5. µCT-determined volumes corresponded with ashing-derived volumes across the maturation stage (ES3 onward). The calculated mineral weight increased from 44.48 ± 11.19 µg (ES3) to 192.12 ± 16.35 µg in mature enamel near the gingival margin (ES8). This represented increases in the % mineral by volume from 26.40% to 95.06%.

Enamel Mineral Density

Filtration and post-processing protocols effectively reduced the influence of a beam-hardening cupping artifact (Appendix Figs. 2, 3). Enamel mineral density increased in a sigmoidal pattern from the secretory (ES1+2) (Ash/BSE) to the late-maturation stage (ES4-8) (Fig. 3). Enamel mineral density peaked at 2.97 ± 0.05 mg HA/mm^3 near the gingival margin (ES8) (µCT/µCT) (Appendix Table 3). Enamel mineral densities in ES 3-5 were statistically similar between ash/BSE and µCT/µCT, but µCT estimates of enamel mineral density were slightly higher. Enamel mineral density discrepancies fell to 2%, 5%, and almost 1% for these same segments when ash/µCT and µCT/µCT enamel mineral densities were compared. This latter comparison highlights the similarity in the mineral content calculation between the ash and the µCT methods.

Inter- and intra-operator variability was minimal (Appendix Table 3). Also, the effect of a VOI radial pixel peel to minimize partial volume boundary effects showed small but significant differences among peel settings (Appendix Fig. 5).

Table. Enamel Volume and Mineral Content by Ashing Combined with BSE Compared with μCT Alone

Stage	ESS	M/LS	EM	MM	MM	LM	LM	LM
Enamel Segment (1 mm)	1	2	3	4	5	6	7	8
"Classic" % Mineral[1]	30	50	75	90	95	95	95	95
BSE n = 3								
Estimated Volume (mm³)								
Mean	0.01165	0.04634	0.07120	0.07324	0.07211	0.06945	0.06860	0.06741
SD	0.00492	0.00204	0.00094	0.00012	0.00024	0.00027	0.00040	0.00176
Expected Mineral Weight[2] (μg)	11.0	73.1	168.5	208.0	216.2	208.2	205.7	202.1
Ashing n = 12								
Measured Mineral Weight (μg)								
Mean	2.27192	16.76667	42.54167	81.16333	133.54167	CND	CND	CND
SD	1.45047	5.82757	12.99094	23.63171	20.95564			
BSE-Ashing								
Estimated Non-mineral Components								
Volume[3] (mm³)	0.00924	0.03571	0.05323	0.04467	0.02757	–	–	–
% Volume[4]	79.31	77.06	74.76	60.99	38.23			
% Mineral[5]	20.69	22.94	25.24	39.01	61.77	–	–	–
Estimated Mineral Weight[6] (μg)	1.54	7.69	14.32	35.18	86.83	–	–	–
MicroCT n = 8								
Computed Volume[3] (mm³)								
Mean	–	–	0.06251	0.06817	0.06509	0.06369	0.06275	0.06477
SD			0.01068	0.00489	0.00462	0.00427	0.00496	0.00574
Computed Mineral Weight (μg)								
Observed	–	–	44.48067	85.91591	133.93322	168.64554	182.44505	192.12524
SD			11.19431	23.91890	17.26646	9.734022	12.12689	16.35890
Non-mineral Components								
Volume (mm³)	–	–	0.04601	0.04001	0.02477	0.01210	0.00709	0.00320
% Volume[4]			73.60	58.69	38.05	19.00	11.30	4.94
Mineral								
% Mineral[5]	–	–	26.40	41.31	61.95	81.00	88.70	95.06

"Classic" % mineral was derived from historical evidence. The expected mineral weight (μg) was derived from the volume and the estimated % mineral. ESS, early secretory stage; MS, mid-secretory stage; LS, late secretory stage; EM, early maturation stage; MM, mid-maturation stage; LM, late maturation stage; and CND, could not dissect, enamel too hard.

Calculations

[1] *"Classic"% mineral* was derived from previously published ashing data.

[2] *Expected mineral weight (μg)* was derived from the measured volumes and the estimated % mineral.

[3] *Estimated non-mineral components* represents organic material and water. It reflects the ratio of observed to expected mineral weight in consideration of the average volume for an enamel slice, according to:

$$\text{Volume non-minerals} = \text{estimated volume} - \left(\frac{\text{measured mineral weight}}{\text{expected mineral weight}} \times \text{estimated volume} \right)$$

[4] *Percentage volume of non-minerals* was calculated as:

$$\% \text{ Volume non-minerals} = \left(\frac{\text{volume non-minerals}}{\text{computed volume}} \times 100 \right)$$

[5] *% Mineral* was estimated as:

$$\% \text{ Mineral} = 100 - \% \text{ Volume non-minerals}$$

For microCT, the measured parameters were volume and mineral density, from which expected mineral weights could be computed as:

$$\text{Weight} = \text{Density} \times \text{Volume}$$

[6] Estimated mineral weight was derived from:

$$\text{Estimated mineral weight} = \left(\frac{\text{measured mineral weight}}{\text{expected mineral weight}} \times \text{measured volume} \right) \times 3156 \times \% \text{ Mineral} \div 100$$
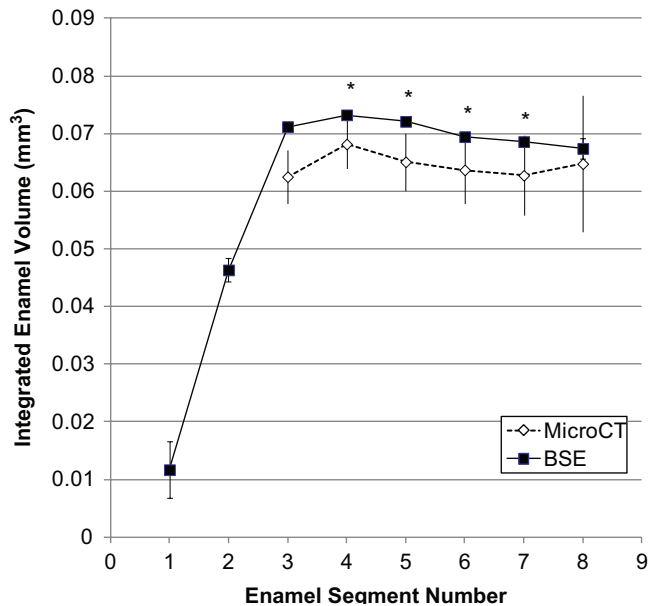
Figure 2. Comparison of integrated incisor enamel volume determined by BSE and μCT. BSE- and μCT-determined volumes of interest show agreement in the course of enamel formation. The earliest enamel mineral detected by μCT was at volume number 3. The volumes in ES 4-7 were statistically different. *p ≤ .05.

Figure 3. Changes in mineral density of forming enamel by ashing (n = 12) combined with BSE or μCT compared with μCT combined with BSE or μCT alone (n = 8). Mineral density was calculated from mineral weight by ashing or μCT combined with enamel volume derived by either BSE or μCT. *p ≤ .05. For numeric mineral density values, see Appendix Table 3.

DISCUSSION

Enamel microdissection was first developed to measure the bulk mineral content in mature enamel (Weidmann *et al.*, 1967) and was later modified to sample developing enamel from rodent incisors (Robinson *et al.*, 1977; Smith and Nanci, 1989). While this technique is the gold standard, it is inherently destructive, is time-consuming (Appendix Table 4), and requires advanced technical skills to process small and frail enamel strips. μCT mineral estimates correspond very well with the ashing technique. Comparisons of results (ash/BSE - μCT/μCT and ash/μCT - μCT/μCT) obtained by 3 different approaches (ash, BSE, μCT) support this argument (Fig. 3). Ash/BSE and μCT/μCT results are statistically similar but showed actual percentage differences of 15%, 12%, and 11% for ES 3-5. These differences in mineral density are the result of volumetric differences between BSE and μCT, since they were reduced to 2%, 5%, and approximately 1% when mineral content estimates from ashing and μCT were divided by μCT-based volumes. Moreover, this similarity suggests that the significant differences observed between μCT/BSE and μCT/μCT densities in segments 7 and 8 originate from volume measurement discrepancies rather than differences in mineral weight.

μCT-based mineral density values showed a sigmoidal pattern through incisor development. The values ranged between 0.7 mg HA/mm³ and 2.97 mg HA/mm³. This range could be measured because we used phantoms with a broad range of densities (Schweizer *et al.*, 2007). It is important to note that the 2.97 mg/mm³ reached in the late maturation stage was lower than previously reported enamel densities based on assumptions about the similarity between enamel and hydroxyapatite (3.15 g/cm³; Angmar *et al.*, 1963) or estimates based on the chemical composition of hydroxyapatite with bound water (2.99 g/cm³; Elliott
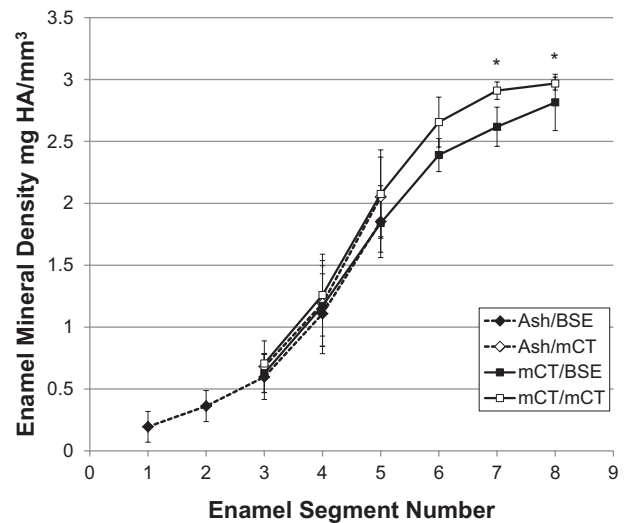
et al., 1998). This peak value, however, is higher than reports on human (Clementino-Luedemann and Kunzelmann, 2006) and rat enamel (Wong *et al.*, 2000), based on aluminum wire reference material. Recently, murine enamel incisor mineral density encased in a methylmethacrylate block was reported to be 2.7 g/cm³, based on calibrations with hydroxyapatite phantoms ranging from 0 to 1.2 g/cm³ (Bronckers *et al.*, 2013). Given this context, the values reported here sit firmly within the range of reported mature enamel densities.

Enamel maturation is a slow process. To reach the final mineral content, ameloblasts devote 65% of their time to the maturation stage. The % mineral in enamel by volume has been reported to range from 86.2% (vol) (Angmar *et al.*, 1963) to 92.9% (vol) (Elliott *et al.*, 1998). These values are greatly influenced by the model used for enamel composition and mineral density (Angmar *et al.*, 1963; Elliott *et al.*, 1998). By combining volumetric measurements from ground enamel sections and calibrated μCT, we bypassed the need for modeling the enamel mineral, arriving at 95.06% mineral by volume in mature enamel.

The influence of beam-hardening on μCT-based measurements of mineral density is well-known (Burghardt *et al.*, 2008; Nazarian *et al.*, 2008; Fajardo *et al.*, 2009; Kovács *et al.*, 2009; Zou *et al.*, 2011; Hamba *et al.*, 2012). Filtration aims to eliminate low-energy photons emitted by the polychromatic source that contribute to the beam-hardening artifact (Zou *et al.*, 2011). Similar to Kovács *et al.* (2009), a 0.5-aluminum filter was used to reduce beam-hardening effects in teeth. The aluminum filter combined with the polynomial correction reduced beam hardening in test images (Appendix Figs. 3, 4) and reduced noise (Meganck *et al.*, 2009). Others have recommended the use of copper or aluminum-copper filters for the analysis of teeth and bones (Meganck *et al.*, 2009; Hamba *et al.*, 2012); however,

these filters increased scan time over four-fold while providing minimal improvement over aluminum in terms of beam-hardening reduction.

Manual contouring of VOIs for μCT analysis is subject to inter- and intra-operator error. VOI precision is critical in these analyses. Values for enamel mineral density were highly repeatable within and between operators. Enamel volume measurements were more sensitive to user error. The greatest variation was found during the early maturation stage due to low quantity and low mineralization of enamel, resulting in poor boundary contrast in μCT images. These results suggest that μCT protocols for contouring tissue interfaces should be performed by a single operator. Future work may require a second set of scan parameters for better imaging of the secretory stage.

μCT offers many advantages over conventional methodologies for estimating enamel density. The time to scan and analyze one sample was approximately 4 hr, a ten-fold reduction in labor time compared with that necessary for microdissection and ashing (Appendix Table 4). μCT can perform volumetric analyses as opposed to 2D estimates of 3D volumes. It is a non-destructive modality, and the same samples can be used for multiple assays. Finally, erupted enamel is the endpoint of enamel formation and is critical to mastication. μCT is capable of analyzing this highly mineralized enamel, which is not feasible with microdissection. However, μCT is limited in its ability to analyze secretory-stage enamel due to the similarity in densities between enamel and dentin. Furthermore, the protocol described here requires that animals be euthanized, which restricts longitudinal studies.

The murine incisor offers an opportunity for the study of genetic mutations in enamel formation that are modeling human amelogenesis imperfecta (Wright *et al.*, 2009). Manual methods such as ashing and the imaging of sectioned samples have been the gold standard for mineral analyses of this tissue. μCT offers a suitable alternative that can accurately quantify mineral content and density while providing many time, cost, and specimen advantages (potentially multiple use). It is concluded that properly calibrated μCT images are as accurate as labor-intensive methods for estimating mineral content and density.

ACKNOWLEDGMENTS

REFERENCES

Angmar B, Carlström D, Glas JE (1963). Studies on the ultrastructure of dental enamel. IV. The mineralization of normal human enamel. *J Ultrastruct Res* 8:12-23.

Bronckers AL, Gueneli N, Lüllmann-Rauch R, Schneppenheim J, Morau AP, Himmerkus N, *et al.* (2013). The intramembrane protease SPPLA is critical for tooth enamel formation. *J Bone Miner Res* 28:1622-1630.

Burghardt AJ, Kazakia GJ, Laib A, Majumdar S (2008). Quantitative assessment of bone tissue mineralization with polychromatic micro-computed tomography. *Calcif Tissue Int* 83:129-138.

Caterina JJ, Skobe Z, Shi J, Ding Y, Simmer JP, Birkedal-Hansen H, *et al.* (2002). Enamelysin (matrix metalloproteinase 20)-deficient mice display an amelogenesis imperfecta phenotype. *J Biol Chem* 277:49598-49604.

Clementino-Luedemann TN, Kunzelmann KH (2006). Mineral concentration of natural human teeth by a commercial micro-CT. *Dent Mater J* 25:113-119.

Elliott JC, Wong FS, Anderson P, Davis GR, Dowker SE (1998). Determination of mineral concentration in dental enamel from x-ray attenuation measurements. *Connect Tissue Res* 38:61-72.

Fajardo RJ, Ryan TM, Kappelman J (2002). Assessing the accuracy of high-resolution x-ray computed tomography of primate trabecular bone by comparisons with histological sections. *Am J Phys Anthropol* 118:1-10.

Fajardo RJ, Cory E, Patel ND, Nazarian A, Laib A, Manoharan RK, *et al.* (2009). Specimen size and porosity can introduce error into microCT-based tissue mineral density measurements. *Bone* 44:176-184.

Feldkamp LA, Davis LC, Kress JW (1984). Practical cone-beam algorithm. *J Opt Soc Am A* 1:612-619.

Fukumoto S, Kiba T, Hall B, Iehara N, Nakamura T, Longenecker G, *et al.* (2004). Ameloblastin is a cell adhesion molecule required for maintaining the differentiation state of ameloblasts. *J Cell Biol* 167:973-983.

Hamba H, Nikaido T, Sadr A, Nakashima S, Tagami J (2012). Enamel lesion parameter correlations between polychromatic micro-CT and TMR. *J Dent Res* 91:586-591.

Hu JC, Hu Y, Smith CE, McKee MD, Wright JT, Yamakoshi Y, *et al.* (2008). Enamel defects and ameloblast-specific expression in Enam knock-out/lacz knock-in mice. *J Biol Chem* 283:10858-10871.

Kovács M, Danyi R, Erdélyi M, Fejérdy P, Dobó-Nagy C (2009). Distortional effect of beam-hardening artefacts on microCT: a simulation study based on an in vitro caries model. *Oral Surg Oral Med Oral Pathol Oral Radiol Endod* 108:591-599.

Lacruz RS, Smith CE, Kurtz I, Hubbard MJ, Paine ML (2013). New paradigms on the transport functions of maturation-stage ameloblasts. *J Dent Res* 92:122-129.

Meganck JA, Kozloff KM, Thornton MM, Broski SM, Goldstein SA (2009). Beam hardening artifacts in micro-computed tomography scanning can be reduced by x-ray beam filtration and the resulting images can be used to accurately measure BMD. *Bone* 45:1104-1116.

Nazarian A, Snyder BD, Zurakowski D, Müller R (2008). Quantitative micro-computed tomography: a non-invasive method to assess equivalent bone mineral density. *Bone* 43:302-311.

Robinson C, Weatherell JA, Hallsworth AS (1971). Variation in composition of dental enamel within thin ground tooth sections. *Caries Res* 5:44-57.

Robinson C, Lowe NR, Weatherell JA (1977). Changes in amino-acid composition of developing rat incisor enamel. *Calcif Tissue Res* 23:19-31.

Schweizer S, Hattendorf B, Schneider P, Aeschlimann B, Gauckler L, Müller R, *et al.* (2007). Preparation and characterization of calibration standards for bone density determination by micro-computed tomography. *Analyst* 132:1040-1045.

Simmer JP, Hu Y, Lertlam R, Yamakoshi Y, Hu JC (2009). Hypomaturation enamel defects in Klk4 knockout/LacZ knockin mice. *J Biol Chem* 284:19110-19121.

Smith CE (1998). Cellular and chemical events during enamel maturation. *Crit Rev Oral Biol Med* 9:128-161.

Smith CE, Nanci A (1989). A method for sampling the stages of amelogenesis on mandibular rat incisors using the molars as a reference for dissection. *Anat Rec* 225:257-266.

Smith CE, Nanci A (1996). Protein dynamics of amelogenesis. *Anat Rec* 245:186-207.

Smith CE, Pompura JR, Borenstein S, Fazel A, Nanci A (1989). Degradation and loss of matrix proteins from developing enamel. *Anat Rec* 224:292-316.

Smith CE, Wazen R, Hu Y, Zalzal SF, Nanci A, Simmer JP, *et al*. (2009). Consequences for enamel development and mineralization resulting from loss of function of ameloblastin or enamelin. *Eur J Oral Sci* 117:485-497.

Smith CE, Richardson AS, Hu Y, Bartlett JD, Hu JC, Simmer JP (2011). Effect of kallikrein 4 loss on enamel mineralization: comparison with mice lacking matrix metalloproteinase 20. *J Biol Chem* 286:18149-18160.

Weidmann SM, Weatherell JA, Hamm SM (1967). Variations of enamel density in sections of human teeth. *Arch Oral Biol* 12:85-97.

Wong FS, Elliott JC, Davis GR, Anderson P (2000). X-ray microradiotomographic study of mineral distribution in enamel of mandibular incisors. *J Anat* 196(Pt 3):405-413.

Wright JT, Hart TC, Hart PS, Simmons D, Suggs C, Daley B, *et al*. (2009). Human and mouse enamel phenotypes resulting from mutation or altered expression of AMEL, ENAM, MMP20 and KLK4. *Cells Tissues Organs* 189:224-229.

Zou W, Hunter N, Swain MV (2011). Application of polychromatic microCT for mineral density determination. *J Dent Res* 90:18-30.